Available online at www.sciencedirect.com
SCIENCE DIRECT®
Journal of Solid State Chemistry 174 (2003) 209–220
JOURNAL OF SOLID STATE CHEMISTRY
http://elsevier.com/locate/jssc

Superspace description of the hexagonal perovskites in the system $Ba_5Nb_4O_{15}$–$BaTiO_3$ as modulated layered structures

Ph. Boullay,[a,*] N. Ténèze,[a] G. Trolliard,[a] D. Mercurio,[a] and J.M. Perez-Mato[b]

[a] *Laboratoire de Sciences des Procédés Céramiques et Traitements de Surface (CNRS UMR6638), Faculté des Sciences et Techniques, Université de Limoges, 123 Av. Albert Thomas, F-87060 Limoges Cedex, France*

[b] *Departamento de Fisica de la Materia Condensada, Facultad de Ciencias, Universidad del Pais Vasco, Apdo. 664, E-48080 Bilbao, Spain*

Received 28 January 2003; received in revised form 17 April 2003; accepted 23 April 2003

Abstract

A general structural model of *B*-site deficient hexagonal layer perovskites $AB_{1-x}X_3$ having no tilting of anion octahedra in consecutive layers is presented. They are described as modulated layered structures using a (3 + 1)-dimensional superspace approach. The presence or not of a given atom along the stacking direction is described in superspace through step-like (crenel) occupational modulation functions. Being essentially composition independent, the model is applicable to any compounds related to this structural type. The component γ of the primary modulation vector $\mathbf{q} = \gamma\mathbf{c}^*$ is connected to the chemical composition by the relation $\gamma = (1 + x)/3$. The model is confirmed and the efficiency of the superspace approach is demonstrated by the structural analysis of some of the hexagonal perovskite found in the system $Ba_5Nb_4O_{15}$–$BaTiO_3$, where long-period intergrowth compounds have been recently identified.

1. Introduction

B-site deficient $A_nB_{n-1}O_{3n}$ hexagonal perovskites based on a mixed cubic and hexagonal close-packed stacking of the AO_3 layers can be described using the Jagodzinski notation [1,2] where a AO_3 layer is denoted h or c whether its neighboring layers are alike or different. In case of a (hhc…c)-type stacking, *B*-site vacancies are often encountered (see, for instance, Ref. [3]) and are usually localized between the two "h-type" AO_3 layers resulting in a completely vacant layer as illustrated in Fig. 1. For simple members (n = integer), these structures possess only blocks of $n - 1$ corner-sharing octahedra (CSO) separated by 1 vacant octahedral layer (VOL). It is known that based on simple members n and $(n + 1)$, intergrowths with more or less long periodicity can be formed as illustrated for oxides in systems like $La_4Ti_3O_{12}$–$LaTiO_3$ [4,5] or $La_4Ti_3O_{12}$–$BaTiO_3$ [6]. These compounds exhibit in all cases a particular deformation of the anionic network consisting in tilts of the oxygen octahedra in neighboring layers. In our recent study of the system $Ba_5Nb_4O_{15}$–$BaTiO_3$ [7], we showed that various ordered intergrowths with (hhc…c)-type sequences can also be formed. These intergrowths consist of the juxtaposition of a number P of perovskite blocks of the type $Ba_5Nb_4O_{15}$ ($n = 5$) [8–10] and 1 perovskite block of the type $Ba_6TiNb_4O_{18}$ ($n = 6$) [11]. They will be further denoted in a compact form as 5^P6^1. The existence of long-period intergrowths of the type 5^P6^1 with compositions $Ba_{11}TiNb_8O_{33}$ (5^16^1) [12], $Ba_{16}TiNb_{12}O_{48}$ (5^26^1) and $Ba_{21}TiNb_{16}O_{63}$ (5^36^1) have been demonstrated by transmission electron microscopy [7]. These complex intergrowths are not only well ordered, but they are also based on a uniform distribution of the minority perovskite blocks (type $n = 6$).

Like the simple terms $Ba_5Nb_4O_{15}$ ($n = 5$) and $Ba_6TiNb_4O_{18}$ ($n = 6$), all the intergrowth compounds of the type 5^P6^1 can be described using the general formula $Ba(Ti,Nb)_{1-x}O_3$ with $x = 1/5$ for $Ba_5Nb_4O_{15}$, $x = 1/6$ for $Ba_6TiNb_4O_{18}$ and, as an example, $x = 2/11$ for $Ba_{11}TiNb_8O_{33}$. This general formula emphasizes the basic perovskite unit, from which all these compounds are derived, where x represents the proportion of *B*-site vacancies per perovskite unit. These compounds are indeed built up with atomic layers of quasi-identical nature for which the average periodicity along the

*Corresponding author. Fax: +33-5-55-45-72-70.
E-mail address: philippe.boullay@unilim.fr (Ph. Boullay).

0022-4596/03/$ - see front matter © 2003 Elsevier Science (USA) All rights reserved.
doi:10.1016/S0022-4596(03)00228-7

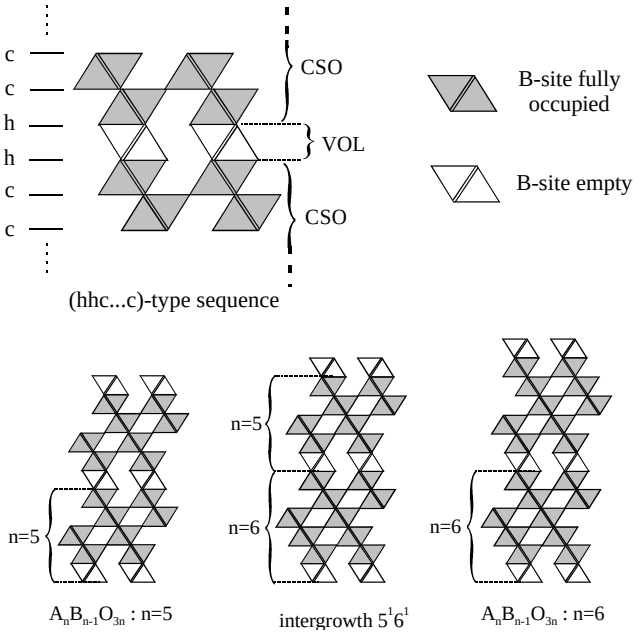

Fig. 1. Schematic representation of (hhc…c)-type *B*-site deficient $A_nB_{n-1}O_{3n}$ perovskites based on a mixed cubic and hexagonal close-packed stacking of the AO_3 layers. The members $n = 5$, $n = 6$ and the compound denoted 5^16^1 resulting from the intergrowth of these two members are represented.

stacking direction is identical but where the stacking sequences differ from one compound to another according to the chemical composition. Based on this observation, some authors [13] have considered the possibility to describe the crystal structures of such compounds using the superspace group formalism. To this respect, a general crystallographic $(3+1)$-dimensional model has recently been proposed and applied to the systems $La_4Ti_3O_{12}$–$LaTiO_3$ [13] and $La_4Ti_3O_{12}$–$BaTiO_3$ [14]. In these compounds, the mentioned systematic octahedra tilting was included in the description through the introduction of a doubled average unit cell along the layer stacking direction, so that the average structure includes two consecutive octahedra. We present here the analogous superspace description as modulated layered structures of the *B*-site deficient hexagonal perovskites that have no such tilting of the anion octahedra, as observed in the system $Ba_5Nb_4O_{15}$–$Ba_6TiNb_4O_{18}$. The advantages over a "classical" 3D crystal structure refinement will be discussed.

2. Description of layered structural families in the superspace group approach

The principle of the superspace modeling consists in simplifying the description by using a basic unit cell (the average structure) that is periodically disturbed by a "modulation". In case of layered structures, the natural way to find this basic unit is to describe the structure in terms of the stacking of atomic layers and for the $Ba(Nb,Ti)_{1-x}O_3$ perovskite type compounds firstly by considering the close-packed stacking of $[BaO_3]$ layers. Within these layers, the in-plane 2D lattice is hexagonal with the parameters $a_h = b_h \approx 5.7$ Å (Fig. 2a). The close-packed stacking of these $[BaO_3]$ layers leads to three type of layers shifted the ones compared to the others according to the way in which they are piled up. Classically, these planes are noted *A*, *B* and *C*. Secondly, the [Ti,Nb] layers (denoted *a*, *b* and *c*) are inserted between the $[BaO_3]$ layers and have a 2D network identical to the one defined by the barium atoms (Fig. 2b). In the cubic sequence, between two $[BaO_3]$ layers of the type *A* and *B*, the inserted [Ti,Nb] layer is of type *c* and thus, for an hypothetical non deficient cubic perovskite $Ba(Ti,Nb)O_3$, one has a *AcBaCb* sequence. In the case of *B*-site deficient hexagonal perovskites, the appearance of hh sequences in the cubic stacking of $[AO_3]$ layers induces the existence of a VOL. The possible succession of layers is thus limited to cases *AcB*, *BaC*, *CbA*, $A \varnothing C$, $B \varnothing A$ and $C \varnothing B$ (where $\varnothing$ represents a VOL). One notices that the layers systematically reproduced along the stacking direction (along *z*) are the $[BaO_3]$ layers (*A*, *B* or *C*). The elementary unit possesses thus a *z*-periodicity corresponding to the average spacing between two $[BaO_3]$ layers, i.e., $c_h \sim 2.35$ Å. The average structure has thus a hexagonal lattice with cell parameters $a_h \sim 5.7$ Å and $c_h \sim 2.35$ Å. It is also seen that the *fcc* stacking (*ABCABC*…) is modified periodically by a *hcp* sequence (*ABAB*, *BCBC* or *CACA*). The VOL can be seen as "defects" in the sequence of the CSO blocks of an hypothetical cubic perovskite $Ba(Ti,Nb)O_3$. The frequency of such *defects* is directly defined by the parameter *x* in the general formula $Ba(Nb,Ti)_{1-x}O_3$, where $x = n(\text{VOL})/n([BaO_3])$ (*x* is then rational and will be further defined like the ratio $x = r/s$ where *r* and *s* are integers). When these *defects* are distributed as uniform as possible, within the restrictions forced by the discrete proportion of VOL and $[BaO_3]$ layers, the intergrowth compound follows a so-called "uniform" stacking sequence [15].

We have shown [7] that the distribution of the *defects* in the stacking sequence of the $Ba(Nb,Ti)_{1-x}O_3$

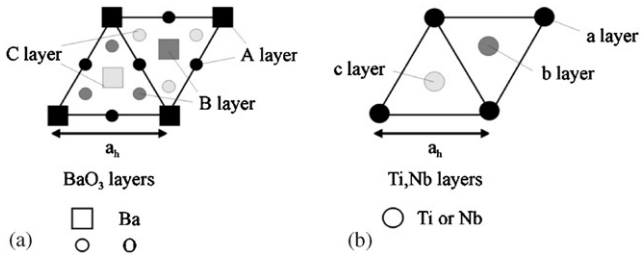

Fig. 2. Schematic representation of the atomic layers involved in the stacking sequences of hexagonal-type perovskite.

compounds is *uniform* (when ordered compounds are observed). That is to say, if one considers a "perturbation" of an hypothetical cubic perovskite $Ba(Ti,Nb)O_3$ by planar defects in the form of VOL, the defects occur in a periodic way and are spaced as far as possible from each other. Hence, for a composition corresponding to $x = 2/11$, the most uniform distribution is 1 fault per 5.5 units perovskites. Considering the discreteness of the stacking of entire perovskite blocks, the uniform sequence results 5 + 6. This principle is very restrictive and leads to a unique uniform sequence for each x value. All possible uniform sequences can be obtained using an arithmetic construction known as the "Farey tree" (Fig. 3) [16,17]. For example, as 2/11 can be decomposed as $2/11 = 1/5 \oplus 1/6$ in the Farey tree scheme, the stacking sequence with $x = 2/11$ is the juxtaposition of one sequence with $x = 1/5$ and one sequence with $x = 1/6$, i.e., $5^1 6^1$.

It has been recently shown that these principles underlie the layer description of many different families of compounds with intergrowth or polytypic features, and they are the basis for their description as modulated structures using the (3 + 1)D superspace formalism [18]. Thus, very efficient (3 + 1)D superspace models have been developed for layer compounds as different as the Aurivillius phases [19], the compound series $Sr_n(Nb,Ti)_nO_{3n+2}$ [20] and the rhombohedral and orthorhombic $A_{1+x}A'_xB_{1-x}O_3$ compounds [21]. The power of the superspace description compared with the conventional 3D approach resides essentially in the fact that a superspace description uses a common symmetry for the whole series of compounds, and the number of structural parameters to be refined is basically independent of the period of the layer stacking sequence.

The transcription of such a layer description into a (3 + 1)D crystallographic model suitable for concrete structure refinements, has been described thoroughly for similar compounds (system $La_4Ti_3O_{12}$–$LaTiO_3$ [13]) and will not be depicted here. The most important point is that the presence or not of a given atom (and hence the occurrence of VOL) along the stacking direction is described in superspace through step-like (crenel) occupational modulation functions for each atom. While the previously depicted layer model is independent of the chemical composition, the component γ of the modulation vector $\mathbf{q} = \gamma \mathbf{c}^*$ can be connected with the chemical composition by the relation $\gamma = (1 + x)/3$. While having the same modulation wave vector, this γ parameter is half the value of the one for the compounds in the systems $La_4Ti_3O_{12}$–$LaTiO_3$ [13] and $La_4Ti_3O_{12}$–$BaTiO_3$ [14], due to the mentioned doubling of the average unit cell in these latter, which is forced by the tilting of consecutive anion octahedra along the c-axis. The absence of such tilting in the $Ba(Nb,Ti)_{1-x}O_3$ compounds also changes the average structure and the superspace group associated to all these structures (given in Table 1), while keeping essentially the same superspace scheme of step occupational functions as in the other systems. The superspace group is here X-$3m1(00\gamma)00$ instead of X-$3c1(00\gamma)00$ for the compounds related to the system $La_4Ti_3O_{12}$–$LaTiO_3$ [13]. The letter X indicates a non-conventional centering in reference to the tables of Janssen [18]. In the present case, the centering corresponds to (2/3,1/3,0,1/3). Some of the (3 + 1)D symmetry operations in Table 1 contain a global phase ϕ. While arbitrary in an incommensurate structure, it takes a fixed value in case of a commensurate modulation, from which depends the resulting conventional 3D space group symmetry. The possible 3D space groups for a given rational composition x can be obtained by applying algebraic rules [18] and are listed in Table 2. This table allows knowing the value of x to limit the choice of the 3D space group to only 3 possibilities that depend on the particular value of the phase ϕ, i.e., the section in superspace, which corresponds to the real space structure.

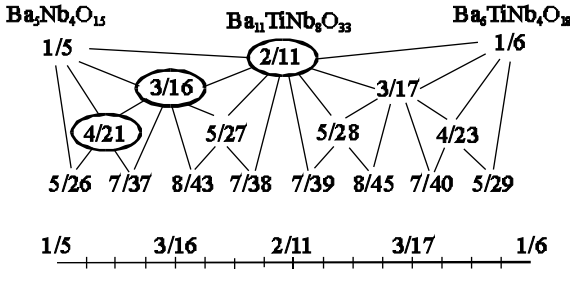

Fig. 3. Representation of the Farey tree series for the pseudo-binary $Ba_5Nb_4O_{15}$–$Ba_6TiNb_4O_{18}$. The members $x = 2/11$, 3/16 and 4/21 are, respectively, decomposed in $1/5 \oplus 1/6$, $1/5 \oplus 1/5 \oplus 1/6$ and $1/5 \oplus 1/5 \oplus 1/5 \oplus 1/6$. The corresponding uniform sequences are thus $5^1 6^1$, $5^2 6^1$ and $5^3 6^1$.

3. Structural analyses of cases $x = 1/6$ and $x = 2/11$: results and discussion

3.1. Experimental

Various intergrowth compounds were synthesized as indicated in details in Refs. [7,12]. All the samples were prepared as white or light yellow colored powders by conventional solid state synthesis, using high purity $BaCO_3$, TiO_2 and Nb_2O_5 oxides. The starting materials were mixed in stoichiometric proportions in an agate mortar and fired at 1400–1500°C in a platinum crucible, for 15–20 h, under ambient atmosphere. The X-ray powder diffraction (XRPD) patterns were obtained with a Siemens D5000 diffractometer ($CuK\alpha_1/K\alpha_2$—graphite monochromator). The diagram was recorded from 15° to 100° (2θ) using a 0.01° step and a time per step of 20 s. The structure refinement was carried out using the software package JANA2000 [22], which allows to

Table 1

Symmetry operations of the superspace group X-3m1(00γ)00 and resulting independent reflection conditions[a]

$\{E, 1\|0\ 0\ 0, 0\}$	$\{1, -1\|0\ 0\ 0, 2\phi\}$
$\{E, 1\|2/3\ 1/3\ 0, 1/3\}$	$\{-3_z+,1\|\ 0\ 0\ 0, 2\phi\}$
$\{E, 1\|1/3\ 2/3\ 0, 2/3\}$	$\{-3_z-,1\|0\ 0\ 0, 2\phi\}$
$\{3_z+,1\|0\ 0\ 0, 0\}$	$\{2_{xy},-1\|0\ 0\ 0, 2\phi\}$
$\{3_z-,1\|0\ 0\ 0, 0\}$	$\{2_x,-1\|0\ 0\ 0, 2\phi\}$
$\{m_{xy}, 1\|0\ 0\ 0, 0\}$	$\{2_y,-1\|0\ 0\ 0, 2\phi\}$
$\{m_x, 1\|0\ 0\ 0, 0\}$	
$\{m_y, 1\|0\ 0\ 0, 0\}$	

hklm: $2h + k + m = 3n$

General structural parameters in the superspace description of the common structure with superspace group X-3m1(00γ)00[b]

Site	x	y	z	x_4	Δ
A	0	0	0.5	0.5	1/3
B	0	0	0	0	$(1-x)/3$
O	0.5	0	0.5	0.5	1/3

[a] $a = b \sim 5.7$ Å, $c = c_h \sim 2.35$ Å and γ is related to the composition variable x in $AB_{1-x}O_3$ by the relation $\gamma = (1+x)/3$.

[b] x_4 and Δ represent the center and width of the crenel function describing the corresponding occupation atomic domain. All the x, y and z atomic coordinates are fixed by symmetry.

Table 2
Space groups for $AB_{1-x}O_3$ commensurate structures described in the superspace group X-3m1(00γ)00 with rational $x = r/s$ and $\gamma = (1+x)/3 = (r+s)/3s$ values, depending on the parity of the denominator s

Condition on s	Condition on ϕ and associated 3D space groups		
$S = 3n$	$\phi = 0$ (mod. 1/s)	$\phi = 1/2s$ (mod. $1/s$)	ϕ arbitrary
	$R\bar{3}m$	$R\bar{3}m$	$R3m$
$S \neq 3n$	$\phi = 0$ (mod. 1/3s)	$\phi = 1/2s$ (mod. $1/s$)	ϕ arbitrary
	$P\bar{3}m1$	$P\bar{3}m1$	$P3m1$

analyze XRPD patterns having a secondary phase and possesses specific tools developed for the (3+1)D superspace treatment of 3D commensurate long-period structures. For both cases the shape of the peaks are described using a pseudo-Voigt function.

It is useful to have in mind a few things regarding the particularities of such refinements [19]:

(i) The atoms in the superspace are represented by atomic domains (further denoted AD), which are, here, defined by discontinuous functions. The occupations are limited by crenel functions where the parameters $x4$ and Δ are, respectively, the center and the width of the crenel (as indicated in Table 1). When combined with a linear displacive function (indicated by its maximal amplitude Az along z in Tables 3 and 4), the resulting sawtooth functions allow a good description of such compounds in a first approximation (see Fig. 4 as an example).

(ii) For a finer description of the atomic displacements, extra displacive Fourier terms can be added (see Tables 3 and 4). To agree with the proposed layered model, the refined structure should be a slightly perturbed solution of the one obtained using only sawtooth functions. As the Fourier terms are not orthogonal to the sawtooth functions, particular cautions should be taken to avoid strong correlations in the refinement. One possibility (used in the present work) is to restrict to zero the lower Fourier terms and use only the higher ones plus the sawtooth function. For a finer description of the structure, one has also to take into account a certain number of satellite reflections, whose order m is limited by the relation $m(\max) = 3s/2$ $(3s = 2n)$ or $m(\max) = (3s-1)/2$ $(3s = 2n+1)$ with s taken from $AB_{1-x}O_3$ $(x = r/s)$.

3.2. $Ba_6TiNB_4O_{18}$: $Ba(Ti, Nb)_{1-x}O_3$ with x=1/6

The case of $Ba_6TiNb_4O_{18}$ is presented here to allow a comparison between two compounds belonging to the same structural family, that is to say $Ba_6TiNb_4O_{18}$ and $Ba_{11}TiNb_8O_{33}$. Figs. 4a and 5a show the x_3-x_4 sections obtained, respectively, by using sawtooth functions alone and after the addition of supplementary displacive modulation functions. The ADs are represented by either straight tilted lines (Fig. 4a) or by undulated cords (Fig. 5a). In each case, the points associated to atomic positions in the 3D physical space are indicated and correspond to a choice of the origin at the section $\phi = 0$.

Table 3
Structure refinement of $Ba(Ti,Nb)_{1-x}O_3$ with $x = 1/6$ ($\gamma = 7/18$) and $\phi = 0$

(a) Fractional coordinates and thermal parameters of the average structure with $a = 5.7777(1)$ Å and $c = 2.3571(1)$ Å

Site	x	y	z	U_{iso}
Ba	0	0	0.5	0.0117(3)
(Ti,Nb)	0	0	0	0.0043(7)
O	0.5	0	0.5	0.0149(16)

(b) Parameters for the sawtooth functions

Site	x_4	Δ	A_z[a]
Ba	0.5	1/3	0.1486(16)
(Ti,Nb)	0	5/18	0.104(3)
O	0.5	1/3	−0.085(5)

(c) Displacive Fourier terms
Ba: $z4\sin = -0.041(2)$
Ti/Nb: $z5\sin = -0.010(3)$
O: $z5\sin = 0.010(6)$ and $x1\sin = 0.0041(14)$

(d) Fourier terms for the occupancy modulation of the *B*-site (Ti,Nb)
Nb: $o1\cos = 0.3(5)$, $o2\cos = -0.7(10)$ and $o3\cos = 0.2(5)$
Ti: link to to the Nb occupancy: 1 Ti for 4 Nb

Reliability factors: $R_{p=}9.36\%$, $R_{wp} = 12.86\%$, GoF = 1.48, $R_{obs} = 4.50\%$, $R_{wobs} = 6.68\%$, $n_{obs} = 195$

Fundamental ($n_{obs} = 17$)	$R_{obs} = 4.40\%$	$R_{wobs} = 5.85\%$
Ordre 1 ($n_{obs} = 30$)	$R_{obs} = 2.90\%$	$R_{wobs} = 3.15\%$
Ordre 2 ($n_{obs} = 25$)	$R_{obs} = 4.44\%$	$R_{wobs} = 4.47\%$
Ordre 3 ($n_{obs} = 31$)	$R_{obs} = 3.50\%$	$R_{wobs} = 6.84\%$
Ordre 4 or sup. ($n_{obs} = 92$)	$R_{obs} = 6.73\%$	$R_{wobs} = 9.70\%$

[a] A_x and A_y are set to zero.

Table 4
Structure refinement of $Ba(Ti,Nb)_{1-x}O_3$ with $x = 2/11$ ($\gamma = 13/33$) and $\phi = 0$

(a) Fractional coordinates and thermal parameters of the average structure with $a = 5.7864(1)$ Å and $c = 2.3575(1)$ Å

Site	x	y	z	U_{iso}
Ba	0	0	0.5	0.0174(4)
(Ti,Nb)	0	0	0	0.0016(6)
O	0.5	0	0.5	0.0038(12)

(b) Parameters for the sawtooth functions

Site	$x4$	Δ	A_z[a]
Ba	0.5	1/3	0.1452(12)
(Ti,Nb)	0	9/33	0.1244(16)
O	0.5	1/3	−0.088(3)

(c) Displacive Fourier terms
Ba: $z4\sin = -0.0191(12)$
Ti/Nb: $z5\sin = -0.0040(16)$
O: $z5\sin = 0.009(3)$ and $x1\sin = -0.002(1)$

(d) Fourier terms for the occupancy modulation of the *B*-site (Ti,Nb)
Nb: $o1\cos = -0.4(2)$, $o2\cos = 0.7(4)$ et $o3\cos = -0.3(2)$
Ti : link to to the Nb occupancy: 1 Ti for 8 Nb

Reliability factors: $R_{p=}9.85\%$, $R_{wp} = 13.77\%$, GoF = 2.79, $R_{obs} = 6.05\%$, $R_{wobs} = 6.29\%$, $n_{obs} = 130$

Fundamental	($n_{obs} = 10$)	$R_{obs} = 6.16\%$	$R_{wobs} = 3.32\%$
Ordre 1	($n_{obs} = 20$)	$R_{obs} = 5.69\%$	$R_{wobs} = 4.07\%$
Ordre 2	($n_{obs} = 17$)	$R_{obs} = 3.60\%$	$R_{wobs} = 6.23\%$
Ordre 3	($n_{obs} = 17$)	$R_{obs} = 5.23\%$	$R_{wobs} = 6.04\%$
Ordre 4 or sup.	($n_{obs} = 66$)	$R_{obs} = 7.47\%$	

[a] A_x and A_y are set to zero.

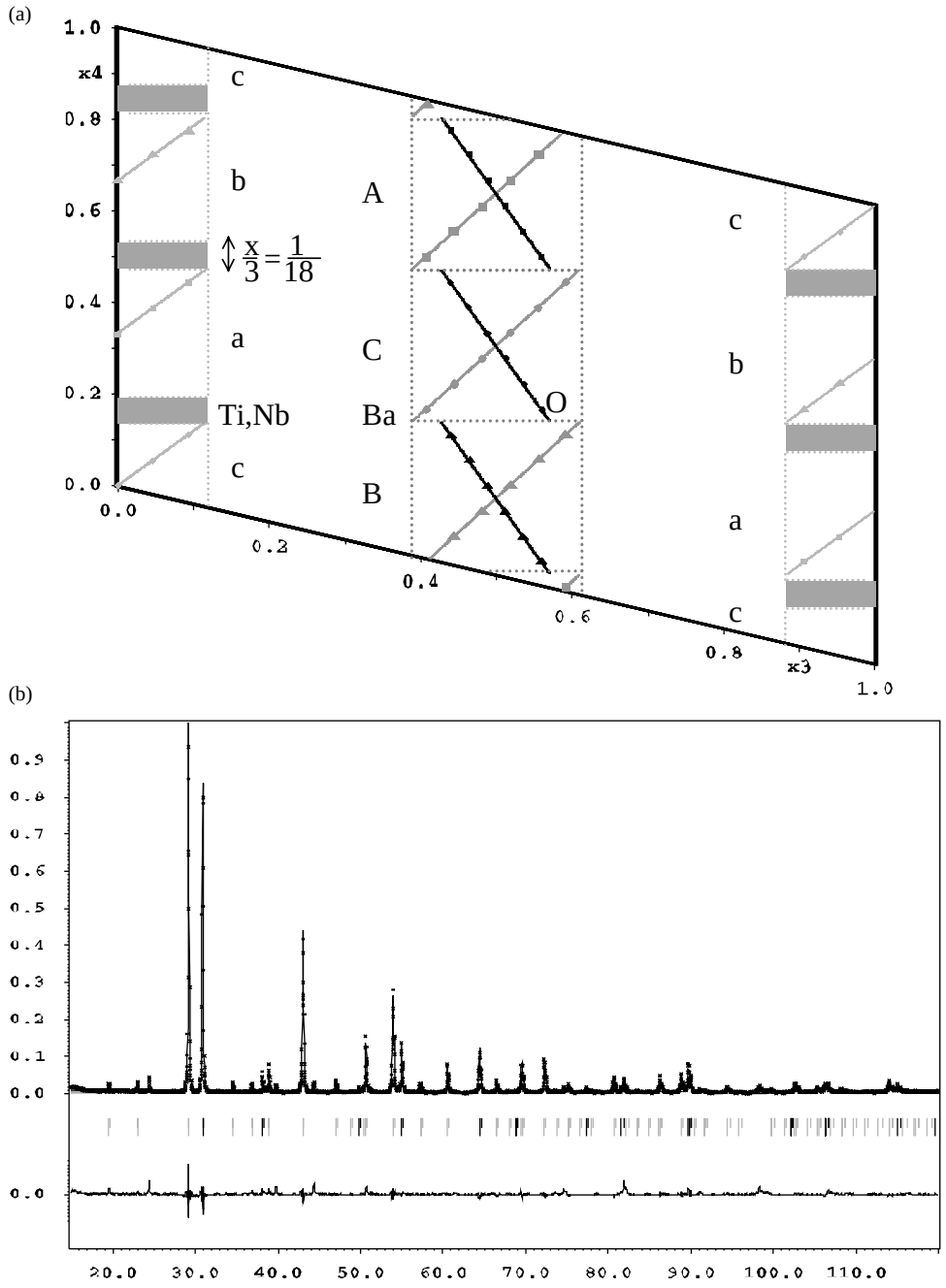

Fig. 4. Results obtained for the refinement of the case $x = 1/6$ with satellites reflections up to order 2 and the use of sawtooth functions only: (a) x_3-x_4 section of the (3+1)D structural model. Atomic domains are represented by straight lines on which the points corresponding to atomic positions in the physical 3D space are represented (section $\phi = 0$). The layers present in the stacking sequence (A, B, C and a, b, c) are indicated by analogy with Fig. 2; (b) observed, calculated and difference plots for the combined XRPD Rietveld refinement of $Ba_6TiNb_4O_{18}$.

The results of the (3+1)D refinement are given in Table 3. The final solution, represented in Fig. 5a, is close to that obtained by using a sawtooth function only. It is also interesting to note that the use of satellite reflections up to the order 2 is already enough to obtain a satisfactory description of the most intense peaks of the XRPD patterns (Fig. 4b). As an indication, the reliability factors obtained for this intermediate refinement are $R_{obs} = 5.71\%$ and $R_{wp} = 22.9\%$ ($n_{obs} = 66$). This confirms that the most intense Bragg peaks are already properly described (low R_{obs}) but the whole pattern profile analysis (high R_{wp}) is still penalized by not considering enough satellite reflections. The final refinement was thus done using satellite reflections up to the order 9 (Fig. 5b), that is to say the same number of reflections was used as in the corresponding 3D commensurate case. For this simple member, the use of (3+1)D refinement did not offer much advantage

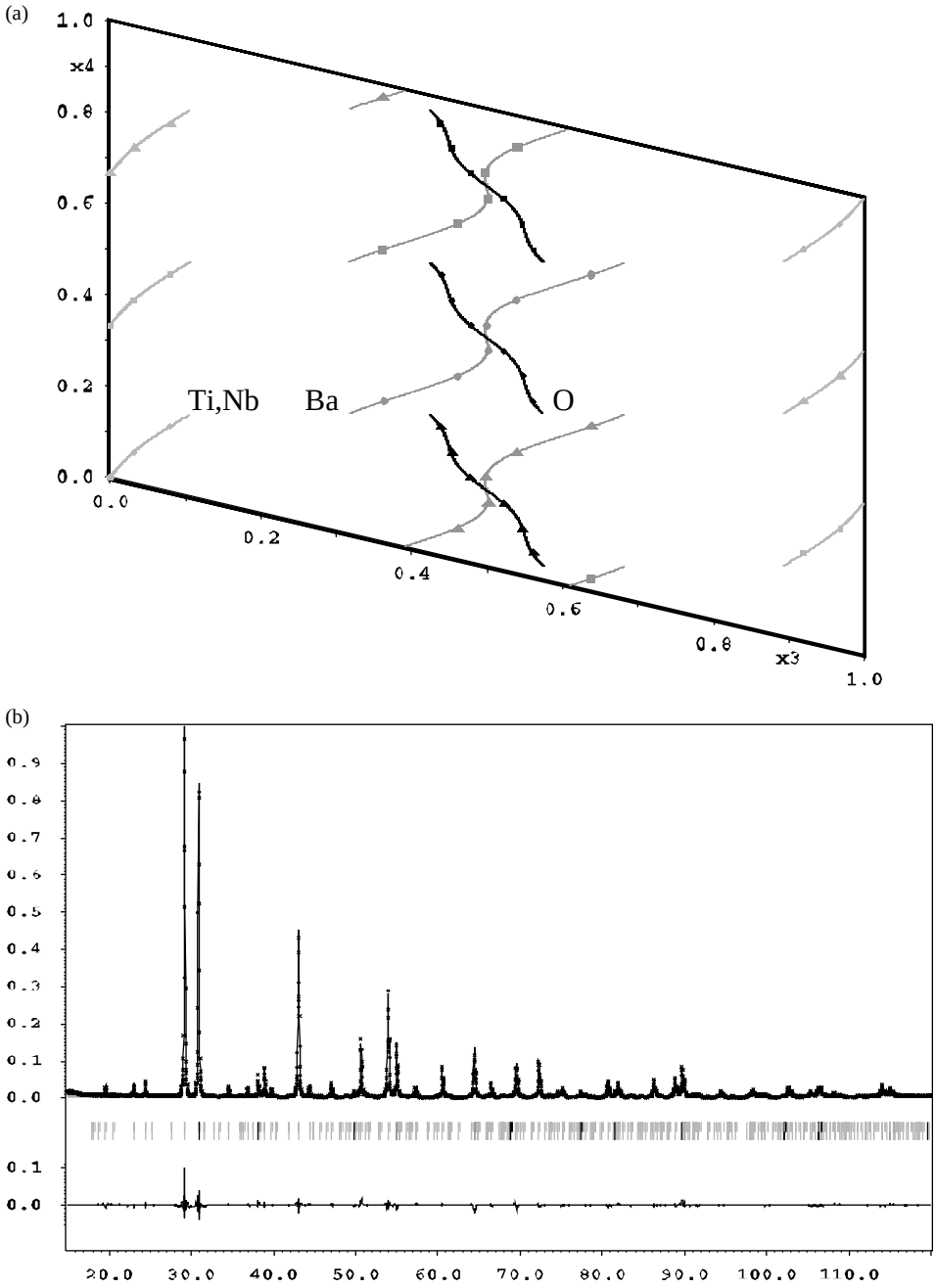

Fig. 5. Results obtained for the refinement of the case $x = 1/6$ with satellites reflections up to order 9: (a) $x_3 - x_4$ section of the (3+1)D structural model. Atomic domains are represented by undulated lines on which the points corresponding to atomic positions in the physical 3D space are represented (section $\phi = 0$); (b) observed, calculated and difference plots for the combined XRPD Rietveld refinement of $Ba_6TiNb_4O_{18}$.

over a conventional 3D refinement. Clearly, the use of the (3+1)D approach will be pertinent for the intergrowth compounds (see below) and especially for the ones having a long periodicity.

3.3. $Ba_{11}TiNB_8O_{33}$ (5^16^1):$Ba(Ti, Nb)_{1-x}O_3$ with x=2/11

The Rietveld analysis of the XRPD patterns obtained in the case of $Ba_{11}TiNb_8O_{33}$ was more difficult for reasons exposed in detail elsewhere [12]. We had to consider effects of micro-structural constraints (see details in Ref. [12]) to obtain a suitable agreement between the observed and calculated diffraction profile for the majority phase $Ba_{11}TiNb_8O_{33}$. Hence, an anisotropic strain broadening was modeled using the tensor method option in JANA2000. Moreover, one secondary phase of the type $n = 6$ had to be introduced. Let us note that this "multiphase" possibility was added recently in JANA2000. For this secondary phase, the

intensities were calculated considering the crystallographic model of the literature [11].

As in the case $x = 1/6$, the simple introduction of the sawtooth functions (only 1 refined parameter per atomic site) and the consideration of a limited number of satellites (up to order $m = 2$ only) already allows to obtain a satisfactory result regarding the modeling of atomic displacements along the stacking direction (Fig. 6). At this stage of the refinement the reliability factors R_{obs} and R_{wp} are, respectively, 4.95% and 19.02% ($n_{obs} = 46$). The use of some additional parameters (4 for the present case) to describe more finely the

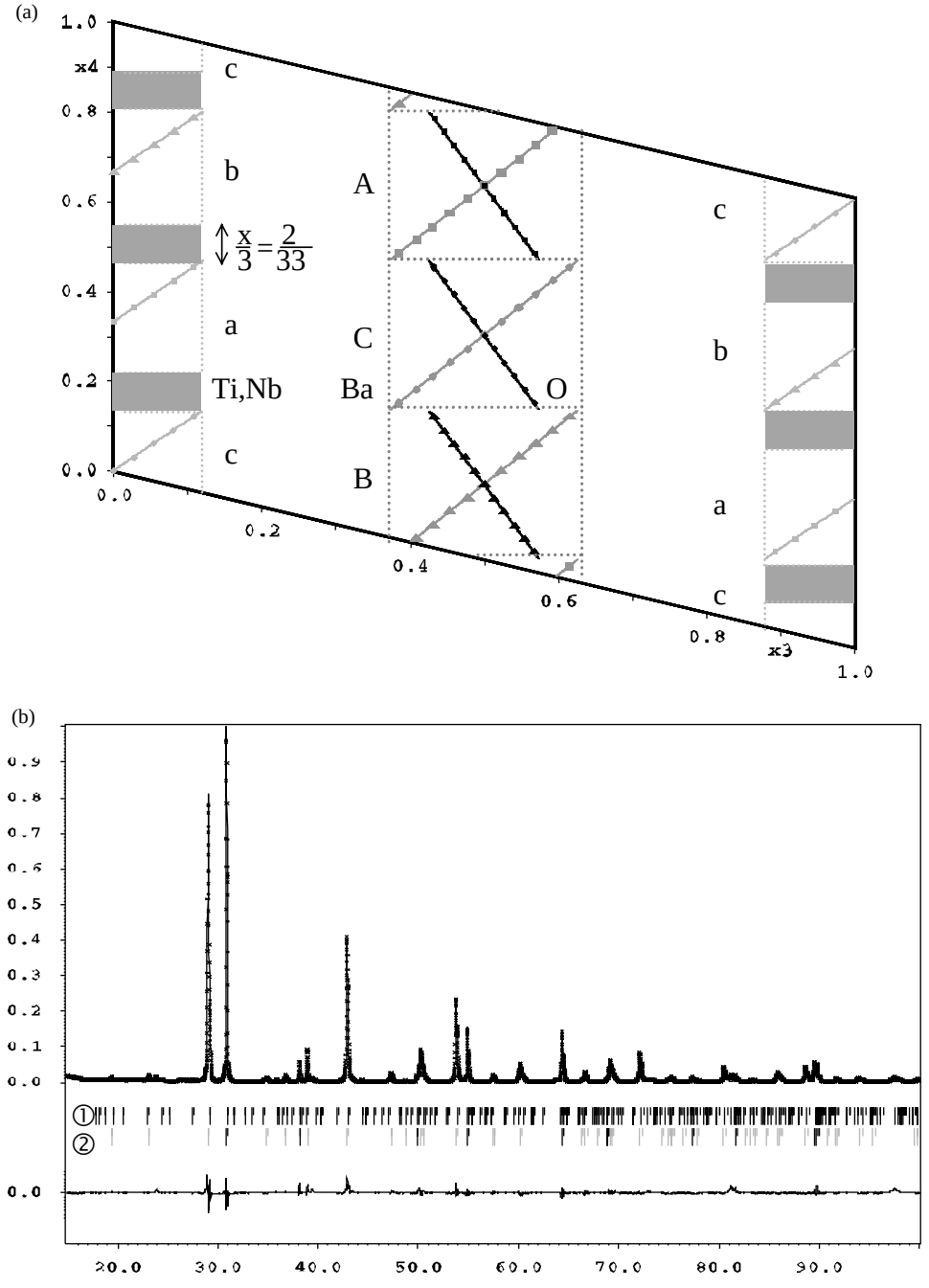

Fig. 6. Results obtained for the refinement of the case $x = 2/11$ with satellites reflections up to order 2 and the use of sawtooth functions only: (a) x_3-x_4 section of the (3+1)D structural model. Atomic domains are represented by straight lines on which the points corresponding to atomic positions in the physical 3D space are represented (section $\phi = 0$). The layers present in the stacking sequence (A, B, C and a, b, c) are indicated by analogy with Fig. 2; (b) final observed, calculated and difference plots for the combined XRPD Rietveld refinement of $Ba_{11}TiNb_8O_{33}$. Marks indicated in lines 1 and 2 correspond, respectively, to reflections from $Ba_6TiNb_4O_{18}$ and $Ba_{11}TiNb_8O_{33}$.

atomic displacements and taking into account a larger number of satellites (up to order $m = 9$), allows to obtain a result as good as the one obtained by the conventional 3D refinement with regard to the statistical reliability factors (see Table 4 and Fig. 7). Note, however, that the number of satellites considered is still far from the maximum allowed (up to order $m = 16$), and therefore the total number of peaks considered was much smaller than in the 3D refinement.

3.4. 3D long period versus (3+1)D commensurate description

In order to easily compare the structural results obtained for the $Ba_{11}TiNb_8O_{33}$ compound, we have transposed the (3 + 1)D structure in its 3D commensurate equivalent with the corresponding inter-atomic distances (see Table 5). The results are in agreement with those obtained by the traditional 3D analysis

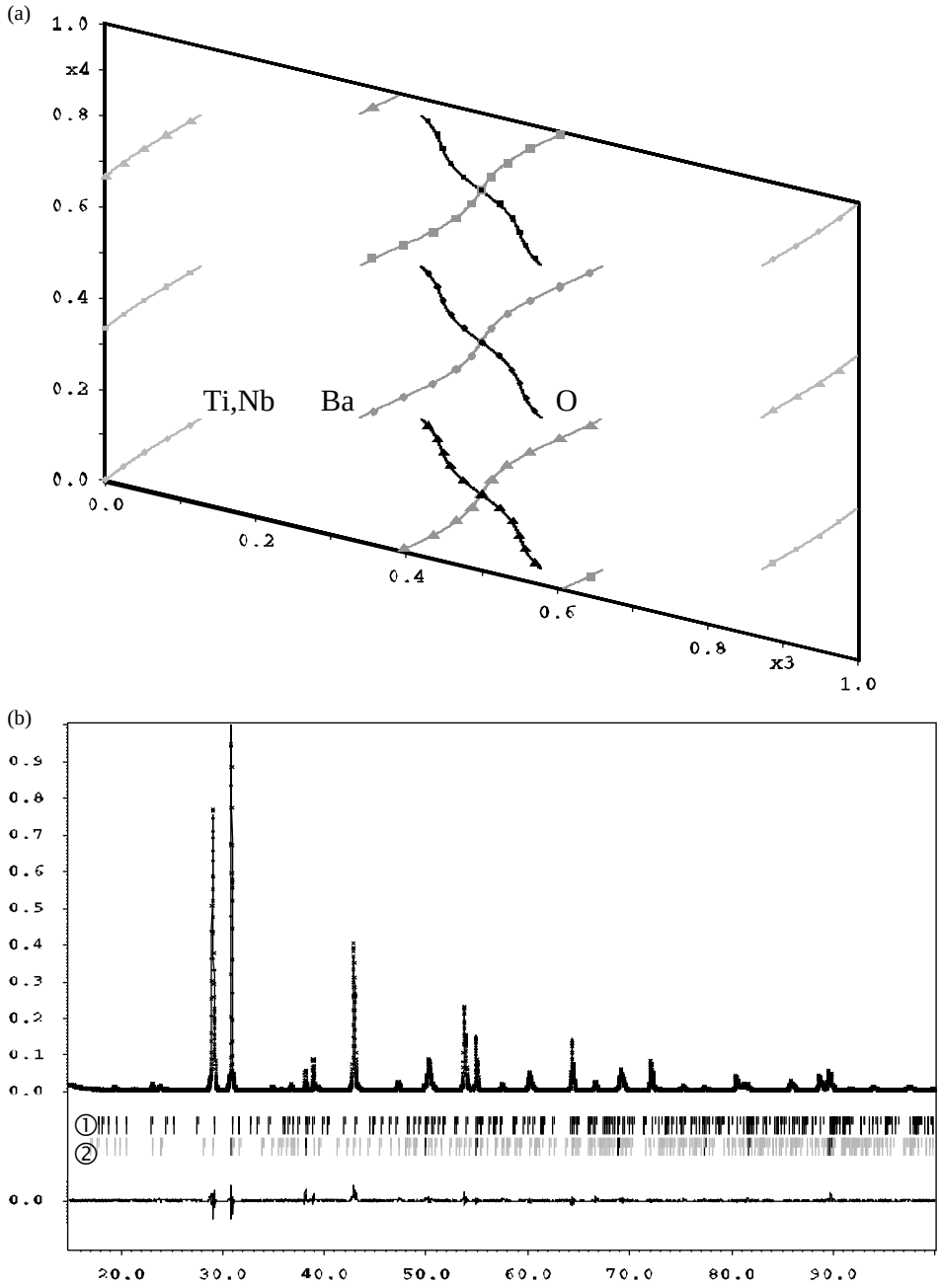

Fig. 7. Results obtained for the refinement of the case $x = 2/11$ with satellites reflections up to order 9: (a) $x_3 - x_4$ section of the (3 + 1)D structural model. Atomic domains are represented by undulated lines on which the points corresponding to atomic positions in the physical 3D space are represented (section $\phi = 0$); (b) final observed, calculated and difference plots for the combined XRPD Rietveld refinement of $Ba_{11}TiNb_8O_{33}$. Marks indicated in lines 1 and 2 correspond, respectively, to reflections from $Ba_6TiNb_4O_{18}$ and $Ba_{11}TiNb_8O_{33}$.

Table 5
$Ba_{11}TiNb_8O_{33}$ structure ($x=2/11$, $\phi=0$) as obtained from the 4D refinement

SG: *R*-3*m* with $a = 5.7864(1)$ Å and $c = 77.799(1)$ Å							
Site	x	y	z	U_{iso}	Occupancy		
(a) Fractional coordinates and thermal parameters							
Ba(1)	0	0	0.5	0.0174(4)	100%		
Ba(2)	0	0	0.1981(1)	0.0174(4)	100%		
Ba(3)	0	0	0.1029(1)	0.0174(4)	100%		
Ba(4)	0	0	0.2532(1)	0.0174(4)	100%		
Ba(5)	0	0	0.0473(1)	0.0174(4)	100%		
Ba(6)	0	0	0.3488(1)	0.0174(4)	100%		
Nb/Ti (1)	0	0	0.1507(1)	0.0016(6)	86%/14% (±4%)		
Nb/Ti (2)	0	0	0.4520(1)	0.0016(6)	85%/15% (±4%)		
Nb/Ti (3)	0	0	0.3974(1)	0.0016(6)	80%/20% (±4%)		
Nb/Ti (4)	0	0	0.3016(1)	0.0016(6)	86%/14% (±4%)		
Nb/Ti (5)	0	0	0	0.0016(6)	85%/15% (±4%)		
O(1)	0.5	0	0.5	0.0038(12)	100%		
O(2)	0.502(2)	0.004(5)	0.1958(3)	0.0038(12)	100%		
O(3)	0.496(2)	−0.008(5)	0.1085(3)	0.0038(12)	100%		
O(4)	0.501(2)	0.001(4)	0.2593(2)	0.0038(12)	100%		
O(5)	0.500(2)	0.001(5)	0.0442(2)	0.0038(12)	100%		
O(6)	0.501(2)	0.001(5)	0.3476(3)	0.0038(12)	100%		
(b) Inter-atomic distances in the coordination sphere of the Ba atoms							
Ba(1)	O(1)	× 6	2.89(1) Å	Ba(4)	O(3)	× 3	2.79(2) Å
	O(2)	× 6	2.83(2) Å		O(4)	× 6	2.93(2) Å
					O(5)	× 3	3.26(2) Å
Ba(2)	O(1)	× 3	2.96(1) Å				
	O(2)	× 6	2.90(2) Å	Ba(5)	O(4)	× 3	2.66(2) Å
	O(3)	× 3	2.69(2) Å		O(5)	× 6	2.90(2) Å
					O(6)	× 3	3.06(2) Å
Ba(3)	O(2)	× 3	3.16(2) Å				
	O(3)	× 6	2.93(2) Å	Ba(6)	O(5)	× 3	2.79(2) Å
	O(4)	× 3	2.79(2) Å		O(6)	× 6	2.89(2) Å
					O(6)	× 3	2.86(2) Å
(c) Inter-atomic distances in the coordination sphere of the *B*-type atoms							
Nb/Ti (1)	O(1)	× 3	2.08(1) Å	Nb/Ti (4)	O(5)	× 3	1.93(2) Å
	O(2)	× 3	1.94(2) Å		O(6)	× 3	2.16(2) Å
Nb/Ti (2)	O(2)	× 3	2.24(2) Å	Nb/Ti (5)	O(6)	× 6	2.00(2) Å
	O(3)	× 3	1.81(2) Å				
Nb/Ti (3)	O(4)	× 3	1.85(2) Å				
	O(5)	× 3	2.28(2) Å				

(see [12]). Concerning the mixed Ti/Nb occupancy of the *B*-sites, the result differs only slightly from that obtained in the 3D analysis. Most significantly it confirms that both Nb and Ti atoms are distributed all over the *B*-sites. The atomic displacements along the stacking direction can be obtained from the x_3-x_4 section of the (3 + 1)D space represented in Fig. 7a (see Ref. [19] for details). A drawing of the corresponding 3D structure ($y0z$ projection) is represented in Fig. 8. Along the stacking direction, the structure of $Ba_{11}TiNb_8O_{33}$ corresponds to the regular intergrowth of one perovskite block of the type $n = 5$ and one perovskite block of the type $n = 6$ separated by one VOL.

In Fig. 7a, the atomic domains of the cations (sites *A* and *B*) and the anions (site O) are tilted in an opposite way. For the Ba and O atomic domains, this corresponds first to the fact that in the "real" structure the O and Ba atoms are not located on a $[BaO_3]$ plane with the same z-coordinate as implied by the idealized starting model (Table 1). More interestingly, this evolution in opposite directions indicates an expansion of the cationic sub-lattice and a compression of the anionic sub-lattice along the stacking direction. Such a structural organization is related to the fact that it exists a deficit in cationic layers compared to an hypothetic cubic perovskite $Ba(Ti,Nb)O_3$. This phenomenon is observed

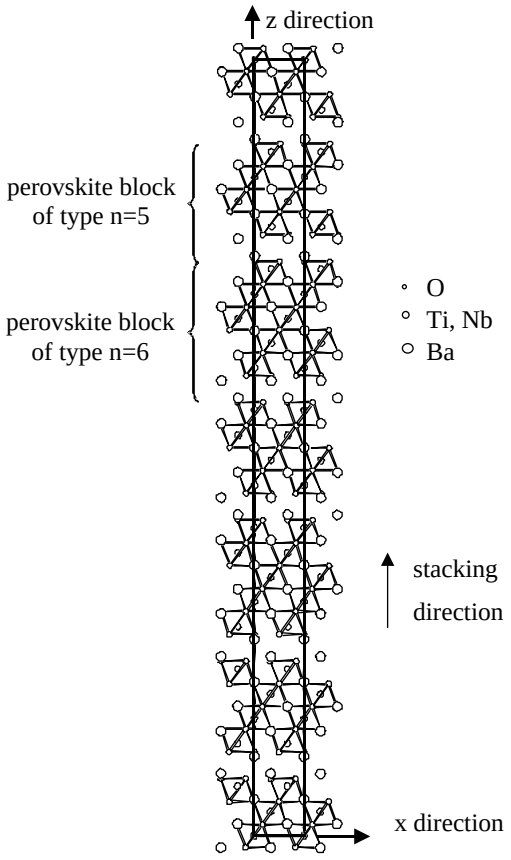

Fig. 8. $Ba_{11}TiNb_8O_{33}$ ($x = 2/11$, SG = R-3m, section $\phi = 0$) structure in projection along **b** as obtained from the (3 + 1)D refinement.

in *B*-site deficient hexagonal perovskites but more generally in all structural families having a deficit in the cationic sub-lattice.

The inclination of the Ba atomic domains represents thus a progressive displacement of the Ba cations along the stacking direction from the center of the cuboctaedral cavity towards the VOL. The closer the cation is to the VOL, the stronger it is displaced from its ideal position. The same applies to the (Ti, Nb) atoms which are increasingly displaced off the center of the octahedral site when one approaches the VOL. Obviously, this structural information is also present in the 3D analysis [12]. The difference here is that these correlations among the atomic positions are not only made obvious, but are also being explicitly used in the structure parametrization, as they are described by the smooth modulation functions of the atomic domains along x_4.

4. Conclusion

Layered long-period compounds (superstructures, polytypoids, intergrowths, etc.) built up with simple units like perovskite are generally commensurable and can thus be studied using a conventional 3D approach. However, for large cell parameters, the number of crystallographic parameters to refine is very large despite the fact that in a first approximation the structure is not very different from that of a cubic perovskite periodically disturbed by a planar defect. This general view corresponds to the way in which the crystallographic approach of these phases is carried out with the help of the superspace formalism. This approach can thus be regarded as a rigorous crystallographic extension of the classical description that would be made of such structural families in any crystal chemistry lessons.

Looking at Figs. 4–7, the similarity of the results obtained for two compounds of the same structural family appears obvious. The solution obtained for one is almost directly transportable to the other. This represents a fundamental difference between the "classic" 3D and the (3 + 1)D superspace approaches. In the 3D approach, the characteristics common to such a structural family are not used in the structure refinement. The conventional 3D description tends to singularize each composition, implying an individual crystallographic processing and a specific space group in each case, whereas the (3 + 1)D superspace description allows a more global processing. The superspace group is unique and, whatever the stacking sequence, the number of structural parameters to refine is identical. Thus in the case of $x = 2/11$, the number of refined positional parameters is 19 in the 3D approach versus only 7 for the (3 + 1)D method. This allows to refine quite easily the structure of a new compound pertaining to a known structural family and presenting a series of intergrowths with long periods depending on the chemical composition.

Although this work was carried out for the case of the series $Ba(Ti,Nb)_{1-x}O_3$, the principles guiding the construction of the corresponding (3 + 1)D superspace model are independent of the chemical composition. Hence, all the arguments developed in the present paper can be used to analyze any *B*-site deficient hexagonal perovskite ($AB_{1-x}O_3$) having analogous structural features.

Acknowledgments

The authors would like to thank Dr. V. Petricek for valuable discussions and for his kindness to provide us modifications of JANA2000 (multiphase refinement in the powder option).

References

[1] H. Jagodzinski, Acta Crystallogr. 2 (1949) 201.

[2] D. Pandey, P. Krishna, Layer stacking in close packed structure, in: A.J.C. Wilson (Ed.), International Tables for Crystallography, Vol. C, Kluwer Academic Publishers, Dordrecht, 1989.
[3] A.F. Wells, Structural Inorganic Chemistry, Oxford University Press, Oxford, 1984.
[4] R. Bontchev, B. Darriet, J. Darriet, F. Weill, G. Van Tendeloo, S. Amelincks, Eur. J. Solid State Inorg. Chem. 30 (1993) 521.
[5] G. Van Tendeloo, S. Amelincks, B. Darriet, R. Bontchev, J. Darriet, F. Weill, J. Solid State Chem. 108 (1994) 314.
[6] G. Trolliard, N. Harre, D. Mercurio, B. Frit, J. Solid State Chem. 145 (1999) 678.
[7] G. Trolliard, N. Ténèze, Ph. Boullay, M. Manier, D. Mercurio, J. Solid State Chem. 173 (2003).
[8] L. Hutchinson, A.J. Jacobson, J. Solid State Chem. 20 (1977) 417.
[9] N. Massa, S. Pagola, R. Carbonio, Phys. Rev. B 53 (1996) 8148.
[10] S. Pagola, G. Polla, G. Leyva, et al., Mater. Sci. Forum 228–231 (1996) 819.
[11] H.C. Van Duivenboden, H.W. Zandbergen, D.J.W. Ijdo, Acta Crystallogr. C 42 (1986) 266.
[12] N. Ténèze, Ph. Boullay, G. Trolliard, D. Mercurio, Solid State Sci. 4 (2002) 1119.
[13] L. Elcoro, J.M. Perez-Mato, R. Withers, Z. Kristallogr. 215 (2000) 727.
[14] V. Petricek, L. Elcoro, J.M. Perez-Mato, J. Darriet, N. Ténèze, D. Mercurio, Ferroelectrics 250 (2001) 31.
[15] S. Amelinckx, D. Van Dyck, Electron Diffraction Techniques, Vol. 2, IUCr Monographs on Crystallography 4, Oxford University Press, Oxford, 1993, p. 309.
[16] J.M. Perez-Mato, M. Zakhour-Nakhl, F. Weil, J. Darriet, J. Mater. Chem. 9 (1999) 2795.
[17] J. Farey, Philos. Mag. 57 (1816) 385.
[18] T. Janssen, A. Janner, A. Looijenga-Vos, P.M. de Wolf, International Tables for Crystallography, Vol. C, Kluwer Academic Press, Dordrecht, 1992.
[19] Ph. Boullay, G. Trolliard, D. Mercurio, L. Elcoro, J.M. Perez-Mato, J. Solid State Chem. 164 (2002) 261.
[20] L. Elcoro, J.M. Perez-Mato, R. Withers, Acta Crystallogr. B 57 (2001) 471.
[21] L. Elcoro, J.M. Perez-Mato, J. Darriet, A. El Abed, Acta Crystallogr. B 59 (2003) 217.
[22] V. Petricek, M. Dusek, The Crystallographic Computing System JANA2000, Institute of Physics, Czech Academy of Sciences, Praha, 2000.